Journal of Zhejiang University-SCIENCE A (Applied Physics & Engineering) 2022 23(5):375-387
www.jzus.zju.edu.cn; www.springer.com/journal/11582
E-mail: jzus_a@zju.edu.cn

Research Article

https://doi.org/10.1631/jzus.A2100401

Vertical temperature gradients of concrete box girder caused by solar radiation in Sichuan-Tibet railway

Tao SHI[1], Xing-wang SHENG[1], Wei-qi ZHENG[1,2]✉, Ping LOU[1,3]

[1]*School of Civil Engineering, Central South University, Changsha 410075, China*
[2]*National Engineering Research Center of High-Speed Railway Construction Technology, Changsha 410075, China*
[3]*MOE Key Laboratory of Engineering Structures of Heavy Haul Railway, Central South University, Changsha 410075, China*

Abstract: Spatial and temporal temperature variations are critical for concrete box girders, and non-uniform temperature distributions induced by solar radiation depend on the structural shapes and shadows cast on them. There have been many studies of temperature distributions and temperature gradients of concrete box girders, but few have considered a high altitude plateau climatic environment. In this study, the nonlinear temperature distributions of concrete box girders in the Sichuan-Tibet railway caused by solar radiation were investigated based on experimental analysis, real-time shadow-selection algorithm, and finite element method. Furthermore, a vertical temperature gradient model of the concrete box girders was obtained. The vertical temperature gradient values first rise, then decrease, and finally rise again from Chengdu to Lhasa, with samples forming a normal distribution. The recommended vertical temperature gradient value was 25 ℃ with a confidence interval of 95%. This provides a reference for the design and maintenance of concrete box girders on the Sichuan-Tibet railway.

Key words: Concrete box girder; Solar radiation; Temperature gradient; Sichuan-Tibet railway; Probability statistics

1 Introduction

In China, the operating mileage of railway networks reached 146000 km by the end of 2020, and several new railway projects are under construction. Among them, the Sichuan-Tibet railway is the most important part of China's 13th Five-Year Plan, which is of great significance to the economic and social development of the Tibet Autonomous Region, Sichuan Province, and other regions in western China (Lu and Cai, 2019). The Sichuan-Tibet railway, at a high altitude linking Chengdu and Lhasa, is in the construction phase. The 1592-km long railway passes through the western Sichuan basin, subsequently climbing 5000 m and running across the Qinghai-Tibet plateau (Fig. 1) (Xue et al., 2021). The railway spans multiple climatic zones, including the subtropical monsoon and alpine climate zones on the Qinghai-Tibet plateau. The effects of the complex and diverse climatic conditions on the construction of the Sichuan-Tibet railway should not be ignored.

Concrete box girders are widely used in the construction of the Sichuan-Tibet railway due to their convenience and low cost. They are subject to thermal actions in the natural environment (such as solar radiation, ambient temperature, and wind speed), causing non-uniform temperature distributions which vary continuously with time and geographical location (Song et al., 2012). The extreme conditions in Tibet, such as the great diurnal temperature variation, intense solar radiation, and high elevation, result in complex non-uniform temperature distributions (Niu et al., 2008; Ma et al., 2011). Therefore, the temperature distributions caused by solar radiation of the concrete box girders in the Sichuan-Tibet railway deserve to be studied in detail.

Some studies have focused on temperature fields and temperature gradients of concrete structures considering environmental conditions. The varying temperature distributions in concrete bridges exposed to complex environmental actions have been studied, based on a temperature experiment involving a

✉ Wei-qi ZHENG, wqzheng@csu.edu.cn
Wei-qi ZHENG, https://orcid.org/0000-0001-7550-5968

Received Aug. 19, 2021; Revision accepted Nov. 22, 2021;
Crosschecked Mar. 23, 2022

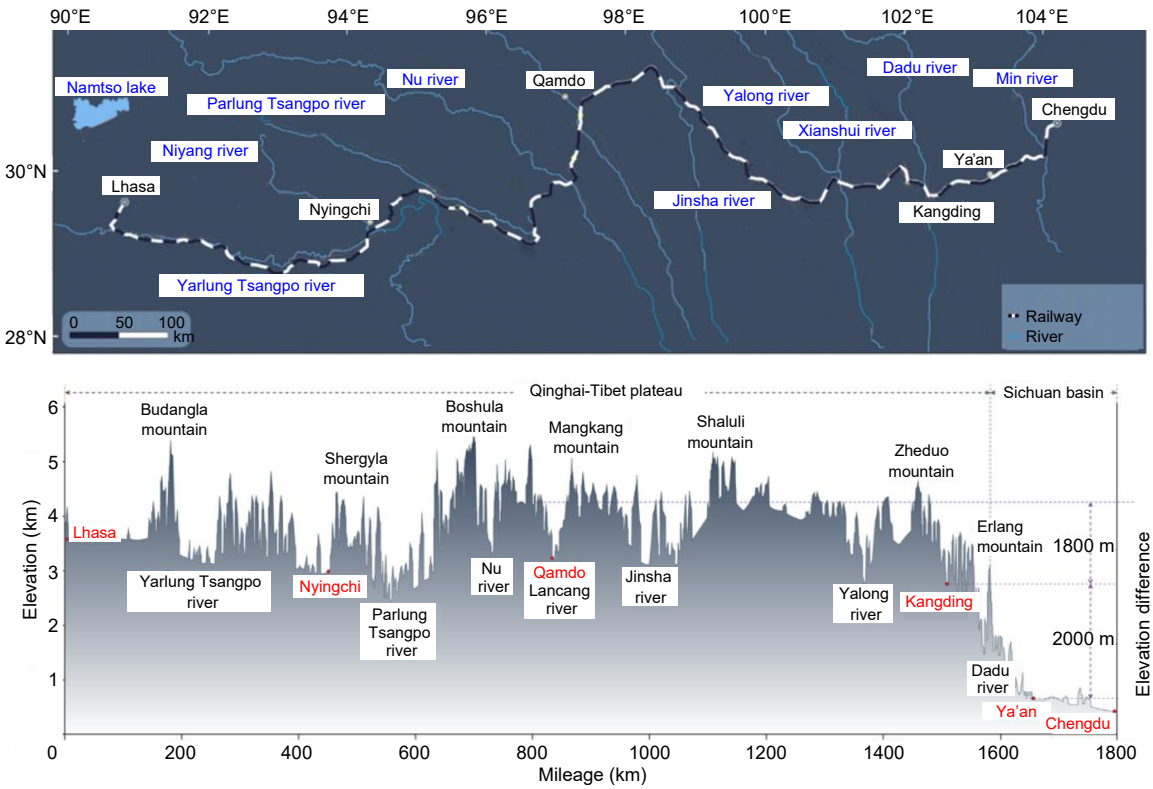

Fig. 1 Diagrammatic maps of Sichuan-Tibet railway (Xue et al., 2021)

full-scale segment of a box-girder bridge (Tayşi and Abid, 2015). A heat transfer analysis of bridge structures has been carried out to calculate temperature distributions, based on a solar radiation algorithm considering the shelter of environmental factors (Chen et al., 2014). Empirical equations used to calculate the temperature gradient values in concrete bridges have been obtained, based on experimental analysis of temperature gradient values (Abid et al., 2016). The design standard values of equivalent linear temperature gradient models and cross-section temperature gradient models have been obtained, based on a stationary binomial probability model (Song et al., 2012). However, because the Sichuan-Tibet railway spans a variety of climate zones under different environmental actions, the temperature gradient values of concrete box girders vary. Thus, the temperature distributions and vertical temperature gradient values of the concrete box girders warrant further detailed study considering the natural environments encountered along the Sichuan-Tibet railway.

In this study, the temperature distributions of the Jiacha No. 2 concrete box girder in the Sichuan-Tibet railway were analyzed, based on experimental temperature data and a finite element model (FEM). The distribution characteristics of the time-varying temperature fields of concrete box girders were studied in detail, and a vertical temperature gradient model of the concrete box girders was proposed. Furthermore, based on a large number of engineering examples and statistical analysis of vertical temperature gradients in the Sichuan-Tibet railway, the recommended vertical temperature gradient value in Sichuan-Tibet railway is proposed.

2 Temperature distributions caused by solar radiation

2.1 Thermal environment and time-varying solar radiation

2.1.1 Thermal environment of a box girder

Concrete structures exchange heat with the natural environment all the time. The forms of heat exchange can generally be divided into solar radiation, convective heat transfer, and radiative heat transfer

(Fig. 2). These three types of heat energy are converted into boundary conditions of heat flux, and the total heat flux on the surfaces of the structure can be expressed by (Tong et al., 2002):

$$q=q_{\mathrm{s}}+q_{\mathrm{c}}+q_{\mathrm{r}}, \tag{1}$$

where q_{s} is the thermal irradiation (J/(m^2·s)), q_{c} is the heat flux of convective heat transfer (J/(m^2·s)), and q_{r} is the heat flux of radiative heat transfer on the structure's surfaces (J/(m^2·s)).

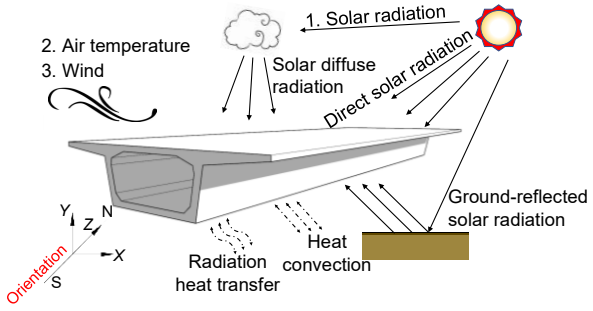

Fig. 2 Thermal environment of the structure

Duffie and Beckman (1991) presented the calculation of the total solar radiation on a tilted surface of a structure. However, due to differences in the type, smoothness, and color of the structural surface materials, and various components in the atmosphere, the solar radiation will not be absorbed completely by the structure. The energy gain of a structure subjected to solar radiation is calculated using

$$q_{\mathrm{s}}=\alpha I_{\mathrm{t}}, \tag{2}$$

where α is the solar radiation absorptivity, and I_{t} is the total solar radiation on a tilted surface of the structure.

The total solar radiation I_{t} on the tilted surface varies due to the sun's movement, which is described in Eq. (3) (Zhang et al., 2020):

$$I_{\mathrm{t}}=I_{\mathrm{bH}}\frac{\cos\theta}{\sin H}+I_{\mathrm{dH}}\left(\frac{1+\cos\beta}{2}\right)+\rho\left(I_{\mathrm{bH}}+I_{\mathrm{dH}}\right)\left(\frac{1-\cos\beta}{2}\right), \tag{3}$$

where I_{bH} is the solar radiation on the horizontal surface, I_{dH} is the diffuse radiation on the horizontal surface, ρ is the reflection coefficient of the ground, θ is the solar incidence angle, β is the tilted angle, and H is the solar altitude angle.

Convective heat transfer occurs between the surfaces and the air. There is a temperature difference between the air and the structure, with air flowing through the structure's surfaces. It is stipulated that heat transfer in the structure's interior is positive, and convection q_{c} is given by Newton's cooling law:

$$q_{\mathrm{c}}=h_{\mathrm{c}}\left(T_{\mathrm{s}}-T_{\mathrm{a}}\right), \tag{4}$$

where T_{s} is the temperature of the structure's surfaces in contact with the air, T_{a} is the ambient temperature, and h_{c} is the convective coefficient (Zhou and Yi, 2013).

The effect of wind speed is considered in the thermal boundaries converted to the heat convection between the surfaces and ambient air. The convective coefficient h_{c} is computed by the empirical formula in Eq. (5) when the wind speed on the surface of the concrete structure is $v\leqslant 5$ m/s (Song et al., 2020):

$$h_{\mathrm{c}}=2.5\left(\sqrt[4]{\left|T_{\mathrm{s}}-T_{\mathrm{a}}\right|}+1.54v\right). \tag{5}$$

The structure's surfaces are exposed to complex environmental actions such as solar radiation, ambient temperature, and windy conditions, emitting electromagnetic waves and radiating and absorbing energy by electromagnetic waves from other objects. The influence of radiative heat transfer on heat flux cannot be ignored. The heat flux of radiative heat transfer on the structure's surfaces is calculated using

$$q_{\mathrm{r}}=A_{\mathrm{l}}\left(G_{\mathrm{a\beta}}+U_{\mathrm{a\beta}}\right)-E_{\mathrm{l}}, \tag{6}$$

where A_{l} is the thermal radiation absorptivity of the materials, $G_{\mathrm{a\beta}}$ is the thermal radiation from the atmosphere on the structure's surfaces, $U_{\mathrm{a\beta}}$ is the heat radiation from the ground to the structure's surfaces, and E_{l} is the energy radiated by the structure.

2.1.2 Time-varying solar radiation conditions

The thermal environment of the structure is directly related to the real-time position of the sun. The solar orientation varies with time, which is described by the longitude and latitude coordinates (λ, φ) of the structure (Meng and Zhu, 2018; Liu et al., 2020a).

According to the relationship between the position of the sun and the structure, Eq. (7) relates the solar altitude angle H to other angles (Fig. 3) as follows (Sheng et al., 2019, 2020a):

$$\sin H=\cos\varphi\cos\delta\cos\omega+\sin\varphi\sin\delta, \tag{7}$$

where δ is the solar declination angle (the angular position of the sun at noon, $-23.45°\leqslant\delta\leqslant23.45°$), φ is the latitude of the structure's surfaces ($-90°\leqslant\varphi\leqslant90°$), and ω is the solar hour angle related to the longitude of the structure's surfaces.

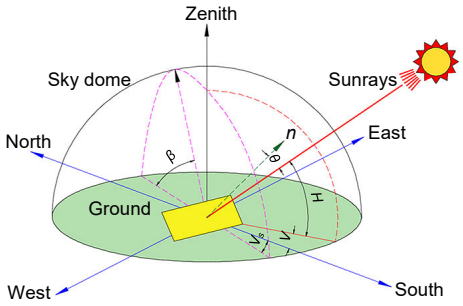

Fig. 3 Relationship between the position of the sun and the structure

In Fig. 3, n is the normal direction of the inclined surface. The azimuth angle V and the solar incidence angle θ are defined as follows:

$$\cos V=\frac{\sin H\sin\varphi-\sin\delta}{\cos H\cos\varphi}, \tag{8}$$

$$\cos\theta=\cos\beta\sin H+\sin\beta\cos H\cos\left(V-V_s\right), \tag{9}$$

where V_s is the surface's azimuth angle.

Based on this, the solar orientation is calculated, and the time-varying solar radiation surfaces of the concrete box girder are obtained using a real-time shadow-selection algorithm, considering the self-shadow area and mutual shadow area (Bourges, 1985; Zhou et al., 2015; Zeng et al., 2018).

Fig. 4 shows that the external surfaces of the right web are self-shadowing areas under the action of light 1, and the sheltered areas of the right web are mutual shadow areas under the action of light 2. As for the self-shadow area, ε is the angle between the vector of the sunlight and the normal vector of the web's external surface. When ε is less than 90°, the web is sheltered from the sunlight, and the external surfaces of the web are unable to be cast.

The selection of the mutual shadow area is as follows. The coordinates of point J are obtained based on the coordinates of the center point W on the external surface element of the web, the solar altitude angle H, and the solar azimuth angle V. The coordinates of point W are obtained from the coordinates of the element node, and the relationship between the point W and the intersection point J is defined as follows (Kim et al., 2009):

$$J_X=f\cos H\sin V+W_X, \tag{10}$$

$$J_Z=f\cos H\cos V+W_Z, \tag{11}$$

$$f=\frac{h-W_Y}{\sin H}, \tag{12}$$

where W_X, W_Y, and W_Z are the X, Y, and Z coordinates of the point W, respectively, J_X and J_Z are the X and Z coordinates of the intersection point J, respectively, f is the distance between the points J and W, and h is the distance from the bottom of the cantilever flange to the bottom flange. If point J falls within area A, the web is sheltered from sunlight by the cantilever flange. Otherwise, the sunlight is not obscured by the cantilever flange. Therefore, the time-varying solar radiation conditions of the concrete box girders are obtained.

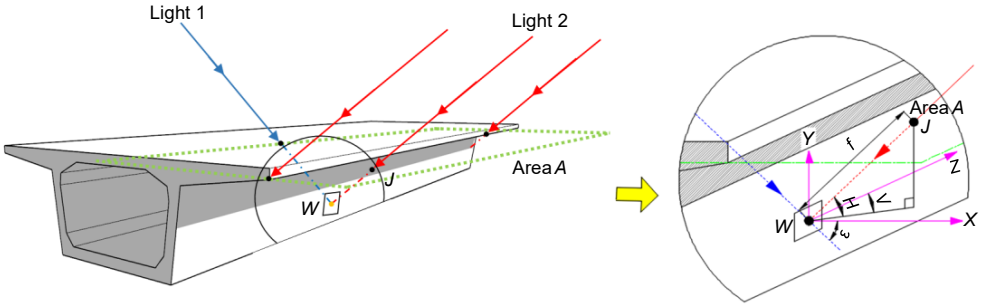

Fig. 4 Area with time-varying solar radiation

2.2 Calculation flow of time-varying temperature distributions

Solar radiation acting on each surface of a concrete box girder differs due to the sun's movement, and the illuminated and shadowed surfaces of the structure have different convective coefficients, affecting the accuracy and reliability of the temperature distribution computations (Abid et al., 2018; Sheng et al., 2020b). Based on this, a method was developed based on a real-time shadow-selection algorithm and finite element method. The calculation flow of temperature distributions induced by solar radiation is shown in Fig. 5.

3 Solar radiation temperature distributions of concrete box girders in the Sichuan-Tibet railway

The temperature distributions caused by solar radiation of concrete box girders are influenced by atmospheric temperature, wind speed, altitude, and weather conditions, varying continuously with time. The temperature of the Jiacha No. 2 concrete box girder was measured on Sept. 2, 2019, to study the time-varying characteristics of the temperature distributions of a concrete box girder on the Sichuan-Tibet railway.

3.1 Experimental progress

The Jiacha No. 2 concrete box girder is located in Jiacha County, Shannan City, Tibet Autonomous Region (29.14°N, 92.59°E). The orientation of the structure is from east to west, and it is located in a mountainous area. The midspan section of the girder was measured, and the measured conditions included the temperatures of the web and top flange. The trends of temperature variation of the web and top flange were investigated and the FEM results were verified (Tayşi and Abid, 2015). The dimensions of the characteristic section and the layout of the sensors are shown in Fig. 6.

From Fig. 6, the temperature sensors T2, T5, and T7 were arranged in the middle of the top flange, middle of the north web, and middle of the south web, respectively. The temperature sensors T1 and T3 were arranged on the top and the bottom edges of the top flange, respectively. The temperature sensors T4 and T6 were arranged on the external edges of the north web and south web, respectively. Based on this temperature experiment, the non-uniform temperature distributions of the concrete box girder were obtained, and the data from Sept. 2, 2019, were used for further research.

3.2 FEM simulation

According to the meteorological data from the China Meteorological Administration (NMIC, 2021), it was cloudy on Sept. 2, 2019, with mid-level cloud, an air temperature of 15.0 to 23.3 °C, and an average wind speed of 1.8 m/s. The calculation parameters in the FEM of the Jiacha No. 2 concrete box girder are listed in Table 1. Wang (2013) proposed that the sky conditions (i.e., weather conditions and cloud form) influence the solar radiation and ground radiation, which are critical for the temperature fields of a concrete box girder. The radiation correction coefficients influenced by the sky conditions are described in Table 2 (Wang, 2013).

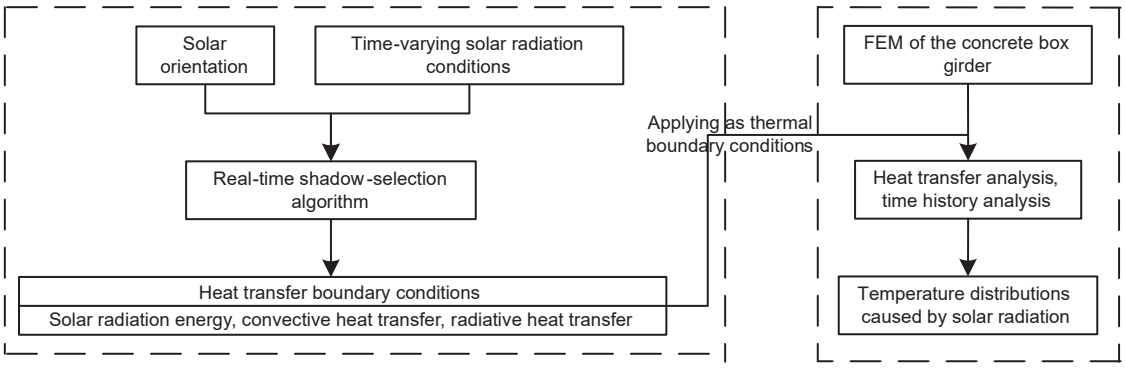

Fig. 5 Calculation flow of temperature distributions caused by solar radiation

Table 1 FEM simulation parameters on Sept. 2, 2019

Parameter	Description
Material	Concrete
Location	Jiacha (29.14°N, 92.59°E)
Wind speed (m/s)	1.8
Ambient temperature (°C)	15.0–23.3
Weather	Cloudy
Cloud form	Mid-level cloud

From Tables 1 and 2, the correction coefficient of solar radiation was 0.4, and the correction coefficient of effective radiation was 0.59 in this study, with the sky condition of cloudy weather and mid-level cloud. It is customary to assume that the minimum ambient temperature (15.0 °C) and the maximum ambient temperature (23.3 °C) occur at 3:00 and 15:00, respectively. The ambient temperature variation is described by Eq. (13) (Dilger et al., 1983).

$$T_{\mathrm{A}}(t)=\frac{1}{2}\left(T_{\mathrm{Amax}}+T_{\mathrm{Amin}}\right)+\frac{1}{2}\left(T_{\mathrm{Amax}}-T_{\mathrm{Amin}}\right)\sin\frac{\pi\left(t-t_{\mathrm{o}}\right)}{12},\tag{13}$$

where T_{Amax} is the maximum ambient temperature, T_{Amin} is the minimum ambient temperature, t is the time, and t_{o} is the parameter representing the time of occurrence of the minimum and maximum ambient temperatures (Dilger et al., 1983). The minimum and maximum ambient temperatures occur at 3:00 and 15:00, respectively, when t_{o}=9.

Based on this, the FEM of the Jiacha No. 2 concrete box girder was established by Solid75 elements using ANSYS 19.0 (Fig. 7).

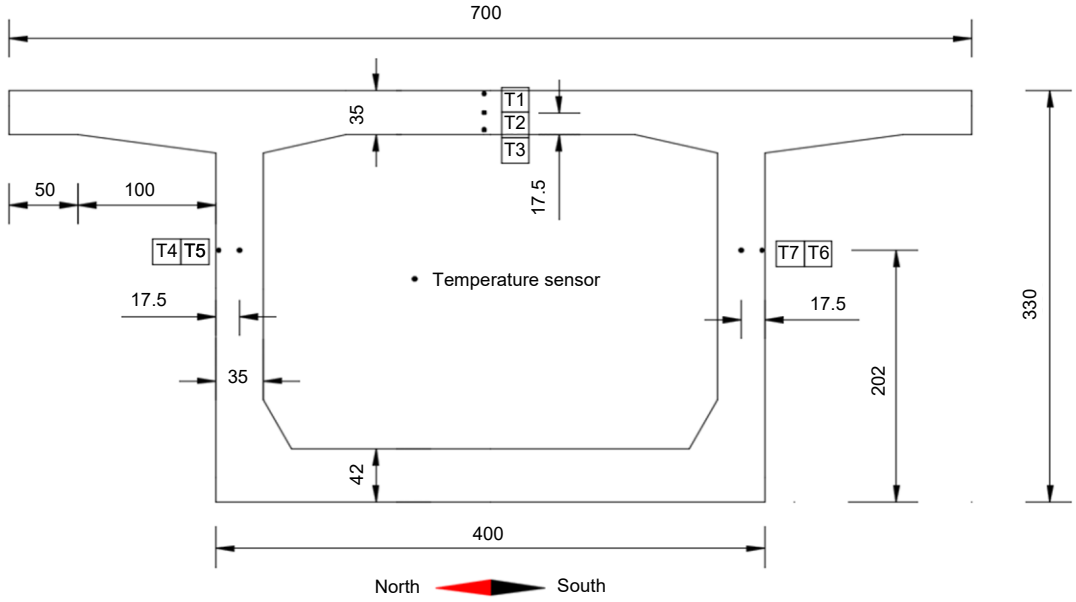

Fig. 6 Dimensions of the characteristic section and the arrangement of sensors (unit: cm)

Table 2 Radiation correction coefficients influenced by the sky conditions

Weather condition	Total cloud cover	Cloud form	Correction coefficient of solar radiation	Correction coefficient of effective radiation
Sunny	0	–	1.00	1.00
Partly cloudy	2.5	High cloud	0.80	0.96
Cloudy	7.5	High cloud	0.40	0.87
		Mid-level cloud	0.40	0.59
Overcast	10	Mid-level cloud	0.19	0.45
		Low cloud	0.19	0.25

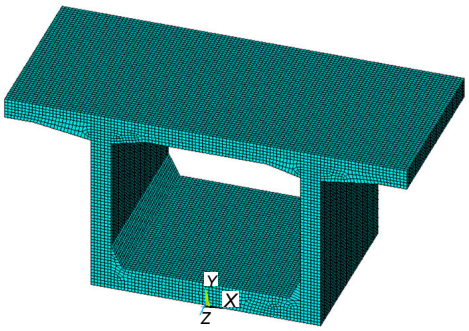

Fig. 7 Finite element model of the Jiacha No. 2 concrete box girder

3.3 Temperature distributions caused by solar radiation

Fig. 8 compares the experimental temperature variations and the finite element analysis results of the above concrete box girder.

From Fig. 8, the trends in the temperature variation of measured and numerical values were almost the same: the temperature of the concrete box girders first decreased, then increased, and finally decreased, during one day. Due to the effect of solar radiation, the temperature variation of the top flange of the girder was the most dramatic. The temperature variation of the web was similar to that of the top flange, and the time of occurrence of the maximum temperature value of the web lagged behind that of the top flange. The temperature distributions induced by solar radiation of the concrete box girder were generally non-uniform and time-dependent. The FEM analysis following the adopted procedure could predict the time-varying temperature variation and temperature distribution accurately, with an average relative error between the measured and calculated data of only 4.46%.

4 Non-uniform temperature distributions and temperature gradient models

4.1 Nonlinear temperature distributions

The Jiacha No. 2 concrete box girder is located in a high plateau climatic zone, with intense solar radiation, small radiation differences, and large temperature differences between day and night. Based on the meteorological data from the China Meteorological Administration, the largest fluctuation of monthly average temperature and the maximum temperature in the summer of 2020 occurred in June. Therefore, June 10, 2020 with sunny weather was selected as the calculation date to simulate the temperature distributions of the concrete box girder. The calculation parameters of the FEM are listed in Table 3, and the temperature fields of the concrete box girder caused by solar radiation are shown in Fig. 9.

From Fig. 9, the temperature values of the concrete box girders varied from 12.39 to 44.28 ℃. Because the ambient temperature was low in the morning, and the short-wave radiation was zero from 22:00 to 5:00, the minimum temperature value occurred at 5:00 on the cantilever end of the concrete box girder. The maximum temperature value occurred at 16:00 on the top flange of the girder due to the effect of prolonged solar radiation. The variation of the temperature value and the temperature difference between the top and bottom flanges in the girder are described in Fig. 10.

As shown in Fig. 10, the temperature values varied from 17.70 to 44.28 ℃ and from 22.37 to 28.25 ℃ on the top and bottom edges of the top flange, respectively. The maximum temperature difference was 19.74 ℃ between the top and bottom edges of the top flange, occurring at 16:00. The trend in temperature variation of the bottom flange was the same as that of the top flange. This phenomenon shows the spatial and temporal variation characteristics of the temperature fields in the concrete box girder. The temperature distributions induced by solar radiation are closely related to the structural characteristics, geographical location, and environmental conditions, which are not universally applicable. Therefore, to be applied in the design and calculation of a concrete box girder in the Sichuan-Tibet railway, it is necessary to obtain a unified temperature gradient model of the girder, which can represent the most unfavorable effect of the solar radiation.

4.2 Vertical temperature gradient models

Based on the analysis of the nonlinear temperature distributions, the maximum temperature differences of the concrete box girder occur at 16:00. The "temperature benchmark" refers to the minimum temperature along the web. The most unfavorable temperature difference in the concrete box girder is the difference between the temperature value at y m from the top flange and the temperature benchmark, at 16:00

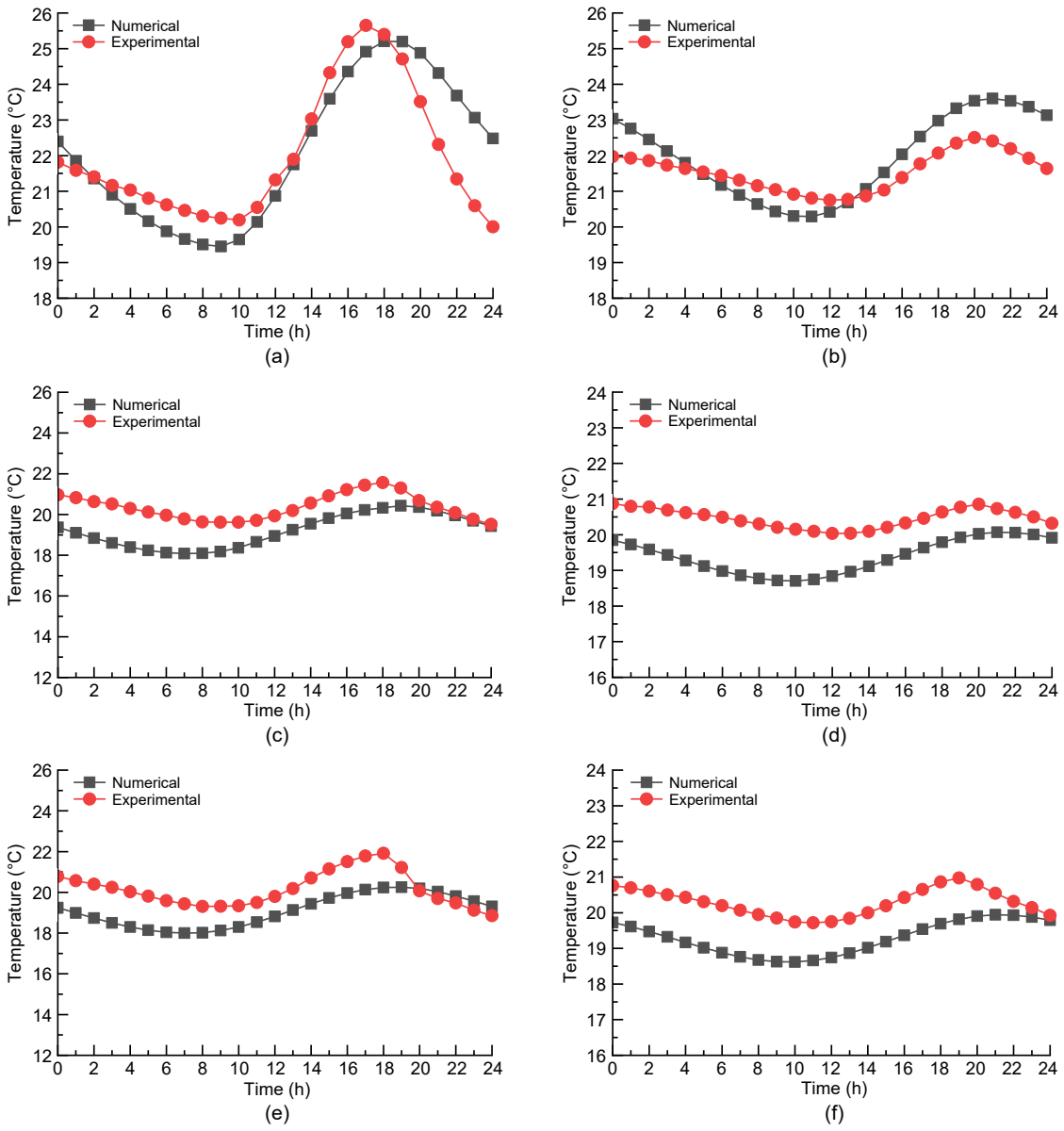

Fig. 8 Experimental data and numerical values of the temperature variations: (a) T1 (top flange); (b) T2 (top flange); (c) T4 (north web); (d) T5 (north web); (e) T6 (south web); (f) T7 (south web)

Table 3 Calculation parameters of the FEM on June 10, 2020

Parameter	Description
Material	Concrete
Location	Jiacha (29.14°N, 92.59°E)
Wind speed (m/s)	1.0
Ambient temperature (°C)	11–24
Weather	Sunny

(Lou et al., 2018). The most unfavorable temperature difference and the fitted temperature gradient model of the concrete box girder are shown in Fig. 11.

From Fig. 11, the vertical temperature gradient model follows the exponential function $T(y)=T_o e^{-ay}$, where T_o is the temperature gradient value (°C) and a is the attenuation coefficient. The vertical temperature gradient model of the Jiacha No. 2 concrete box girder in the Sichuan-Tibet railway is described by

$$T(y)=25e^{-5y}. \tag{14}$$

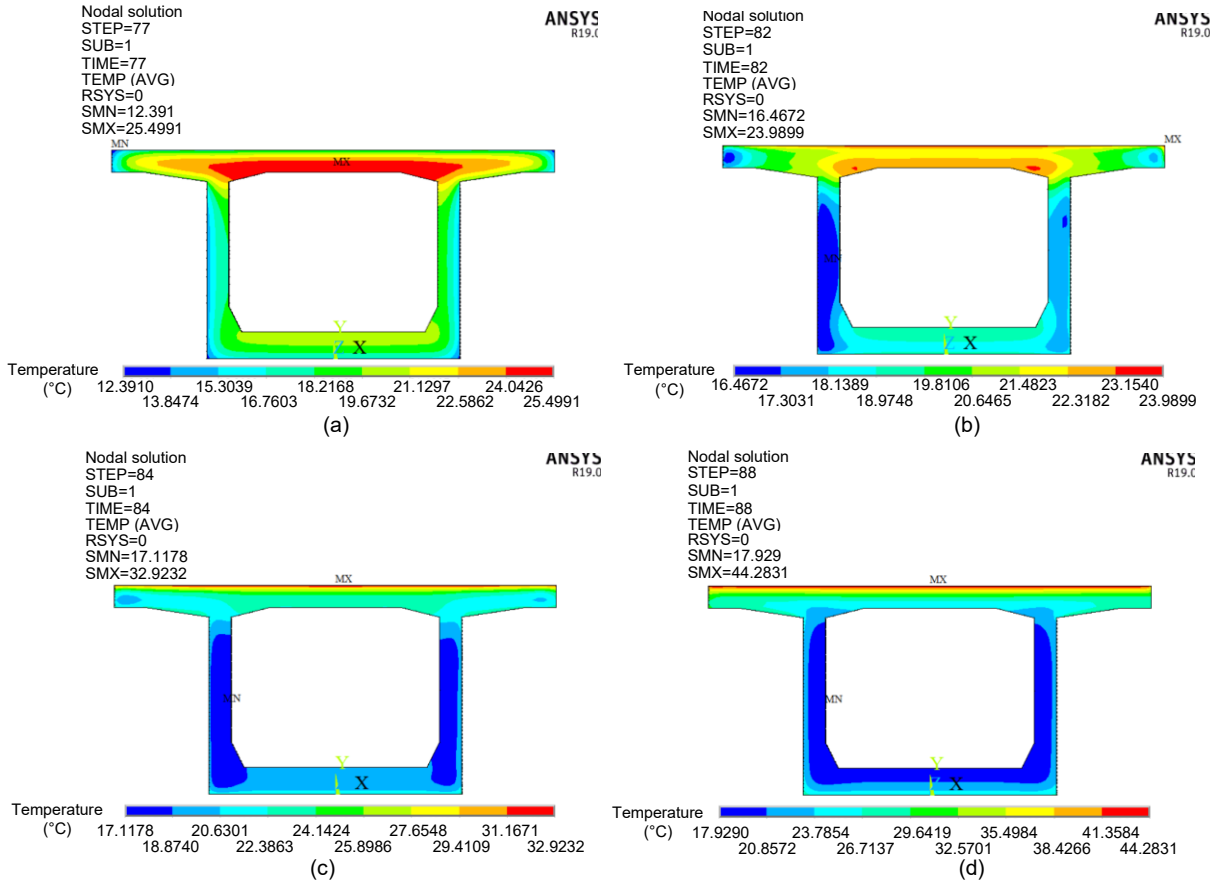

Fig. 9 Unfavorable temperature fields of the concrete box girder: (a) 5:00; (b) 10:00; (c) 12:00; (d) 16:00

5 Discussion

5.1 Variation of vertical temperature gradient values in the Sichuan-Tibet railway

Based on the above vertical temperature gradient model, a series of FEM analyses of concrete box girders in the Sichuan-Tibet railway were carried out, and the trend in the variation of the vertical temperature gradient values was explored. The variation of vertical temperature gradient values of the box girders is shown in Fig. 12.

From Fig. 12, the vertical temperature gradient values vary because the Sichuan-Tibet railway spans a variety of climatic zones. The vertical temperature gradient values first rise, then decrease, and finally rise from Chengdu to Lhasa. The vertical temperature gradient values rise with increasing diurnal temperature differences. The diurnal temperature difference of 13 ℃ in Litang is the largest in the Sichuan-Tibet railway, and the vertical temperature gradient value of the concrete box girder in Litang reaches the peak value of 25.0 ℃.

5.2 Statistics of vertical temperature gradient values in Sichuan-Tibet railway

Based on the above analysis, the vertical temperature gradient values ΔT of the concrete box girders at 100 different sites in Sichuan-Tibet railway were calculated (Fig. 13).

Fig. 13 shows the vertical temperature gradient values form a “bell-shaped distribution”. The Shapiro Wilk test was used to test the null hypothesis that the sample random variable ΔT comes from a normal distribution (Royston, 1992; Razali and Wah, 2011; Hanusz and Tarasińska, 2015). The p-value of 0.34 was higher than the significance level of 0.05. Therefore, the null hypothesis of normality cannot be rejected. Moreover, the normal quantile plot was used to visualize the extent to which the sample random variable ΔT was distributed normally in Fig. 14 (Tan et al., 2004).

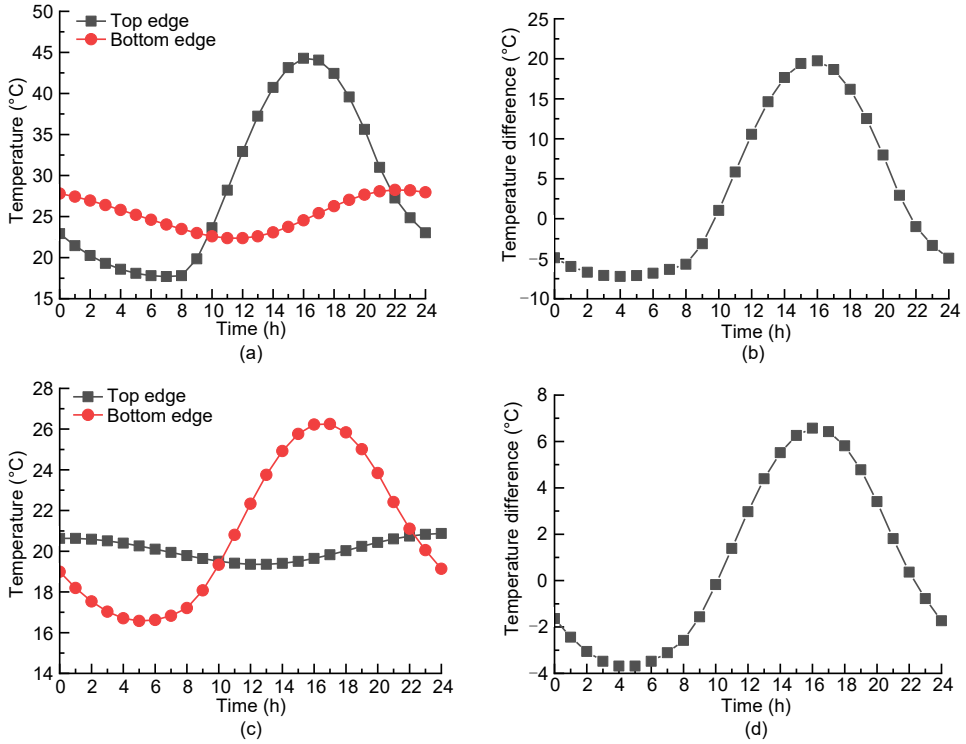

Fig. 10 Temperature variations of the top and bottom flanges: (a) temperature value of top flange; (b) temperature difference of top flange; (c) temperature value of bottom flange; (d) temperature difference of bottom flange

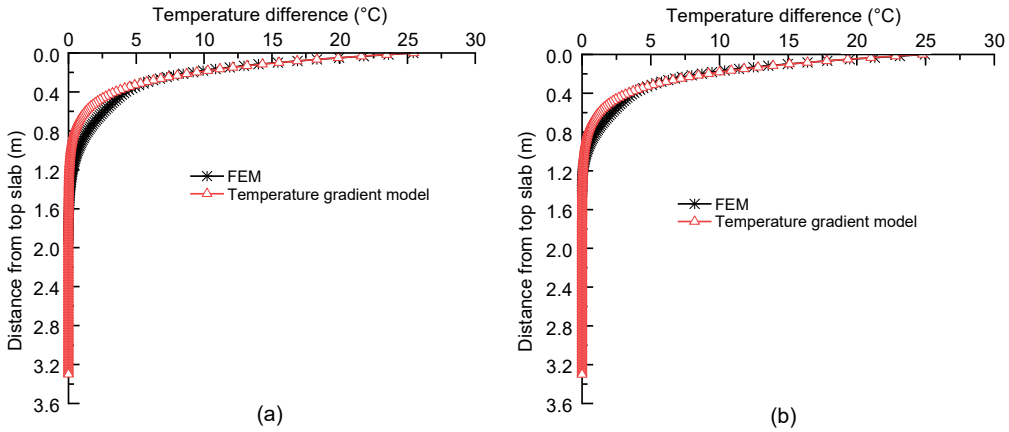

Fig. 11 Maximum temperature differences and the fitted temperature gradient model: (a) south web; (b) north web

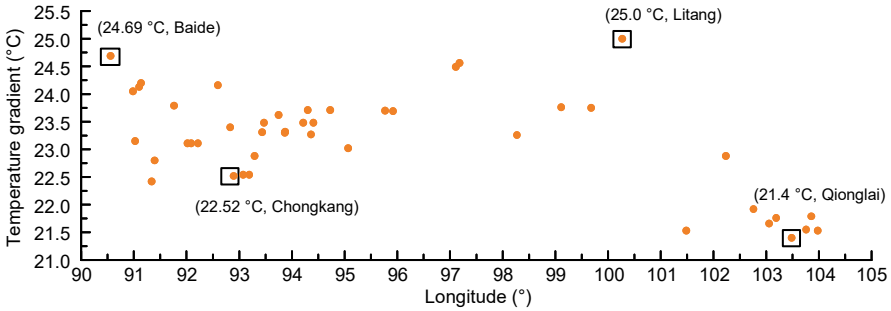

Fig. 12 Vertical temperature gradient values of concrete box girders in the Sichuan-Tibet railway

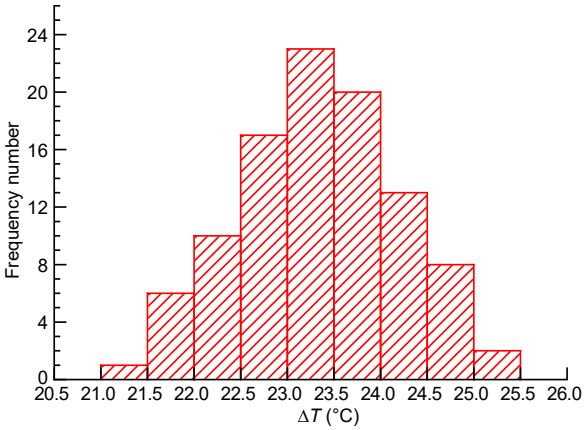

Fig. 13 Histogram of the vertical temperature gradients

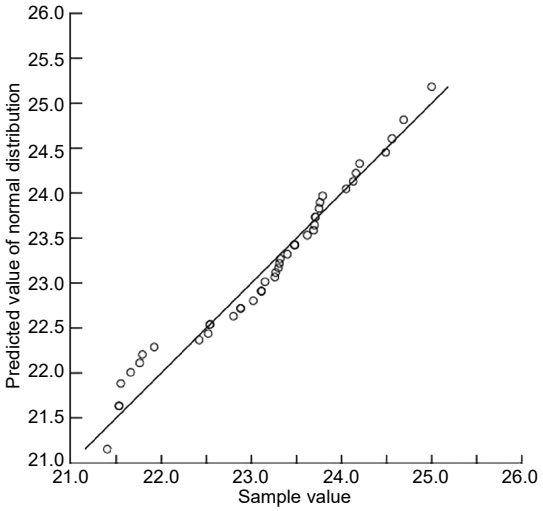

Fig. 14 Normal quantile plot (Tan et al., 2004)

From Fig. 14, the sample random variable ΔT was normally distributed, with the normal quantile plot approximating a diagonal straight line. Therefore, the sample random variable ΔT comes from a normal distribution, and the normal distribution equation is expressed as

$$f(x)=\frac{A}{w\sqrt{\frac{\pi}{2}}}\mathrm{e}^{-2\left(\frac{x-x_c}{w}\right)^2}, \tag{15}$$

where A=50.73, w=1.83, and x_c=23.36.

Based on Eq. (15), the sample random variable ΔT coming from the normal distribution is described simply by

$$\Delta T\sim N(23.36, 0.837). \tag{16}$$

From the analysis of the normal distribution equation, the cumulative probability density curve of the vertical temperature gradient value ΔT was calculated (Fig. 15).

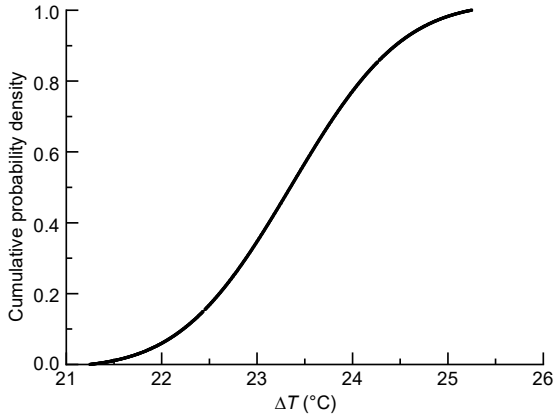

Fig. 15 Cumulative probability density curve of the vertical temperature gradients

From Fig. 15, the distribution of cumulative probability density of the vertical temperature gradients ΔT, can be described as an S-shaped curve. The vertical temperature gradient values with various confidence intervals are obtained. Table 4 shows the vertical temperature gradient values with confidence intervals of 98%, 95%, or 90%.

Table 4 Vertical temperature gradient values based on probability statistics

Vertical temperature gradient (°C)	Confidence interval (%)
24.97	98
24.72	95
24.45	90

As shown in Table 4, the vertical temperature gradient value in Sichuan-Tibet railway is 24.72 °C with a confidence interval of 95%. The representative vertical temperature gradient value of a concrete box girder in Lhasa was 24.678 °C (Liu et al., 2020b), verifying that the estimated value was reasonable. The vertical temperature gradient value of 24.72 °C is larger than that of 20 °C in the China highway bridges design code (MOT, 2015), and smaller than that of 25 °C in the China railway bridges design code (NRA, 2017). Based on the complex and diverse climatic conditions in Sichuan-Tibet railway, a vertical temperature gradient value of 25 °C of a concrete box girder in the Sichuan-Tibet railway is recommended.

6 Conclusions

In this study, the nonlinear temperature distributions of concrete box girders in the Sichuan-Tibet railway caused by solar radiation were investigated. A vertical temperature gradient model of the concrete box girder was obtained and the trend in the variation of the vertical temperature gradient values was analyzed. A recommended vertical temperature gradient value of the concrete box girders in the Sichuan-Tibet railway is proposed. The main conclusions of this study were as follows:

1. Based on a temperature experiment and finite element analysis, the temperature variation of the Jiacha No. 2 concrete box girder in the Sichuan-Tibet railway was analyzed. FEM analysis verified that the adopted procedure could predict the time-varying temperature distributions accurately.

2. The nonlinear temperature distributions of the concrete box girders in the Sichuan-Tibet railway caused by solar radiation were studied, and a vertical temperature gradient model was obtained, which is described by $T(y)=25e^{-5y}$.

3. The vertical temperature gradient values first rise, then decrease, and finally rise from Chengdu to Lhasa and the samples ΔT come from a normal distribution, shown as $\Delta T \sim N(23.36, 0.837)$.

4. The recommended vertical temperature gradient value in the Sichuan-Tibet railway is 25 °C with a confidence interval of 95%, providing a reference for the design and maintenance of concrete box girders in the Sichuan-Tibet railway.

Acknowledgments

This work is supported by the National Natural Science Foundation of China (Nos. 52078488 and 52078501), the Project of National Railway Administration of China (No. KF2019-018), and the Science and Technology Research and Development Plan of China State Railway Group Co., Ltd. (No. L2021G006).

Author contributions

Tao SHI was responsible for establishing the finite element model and part of the paper writing, Xing-wang SHENG for the experimental setup, Wei-qi ZHENG for theoretical analysis and part of the paper writing, and Ping LOU for the literature review.

Conflict of interest

Tao SHI, Xing-wang SHENG, Wei-qi ZHENG, and Ping LOU declare that they have no conflict of interest.

References

Abid SR, Tayşi N, Özakça M, 2016. Experimental analysis of temperature gradients in concrete box-girders. *Construction and Building Materials*, 106:523-532. https://doi.org/10.1016/j.conbuildmat.2015.12.144

Abid SR, Mussa F, Tayşi N, et al., 2018. Experimental and finite element investigation of temperature distributions in concrete-encased steel girders. *Structural Control and Health Monitoring*, 25(1):e2042. https://doi.org/10.1002/stc.2042

Bourges B, 1985. Improvement in solar declination computation. *Solar Energy*, 35(4):367-369. https://doi.org/10.1016/0038-092X(85)90144-6

Chen B, Sun YZ, Wang GJ, et al., 2014. Assessment on time-varying thermal loading of engineering structures based on a new solar radiation model. *Mathematical Problems in Engineering*, 2014:639867. https://doi.org/10.1155/2014/639867

Dilger WH, Ghali A, Chan M, et al., 1983. Temperature stresses in composite box girder bridges. *Journal of Structural Engineering*, 109(6):1460-1478. https://doi.org/10.1061/(asce)0733-9445(1983)109:6(1460)

Duffie JA, Beckman WA, 1991. Solar Energy of Thermal Process, 2nd Edition. John Wiley & Sons, New York, USA.

Hanusz Z, Tarasińska J, 2015. Normalization of the Kolmogorov-Smirnov and Shapiro-Wilk tests of normality. *Biometrical Letters*, 52(2):85-93. https://doi.org/10.1515/bile-2015-0008

Kim SH, Cho KI, Won JH, et al., 2009. A study on thermal behaviour of curved steel box girder bridges considering solar radiation. *Archives of Civil and Mechanical Engineering*, 9(3):59-76. https://doi.org/10.1016/S1644-9665(12)60218-0

Liu J, Liu YJ, Zhang GJ, et al., 2020a. Prediction formula for temperature gradient of concrete-filled steel tubular member with an arbitrary inclination. *Journal of Bridge Engineering*, 25(10):04020076. https://doi.org/10.1061/(ASCE)BE.1943-5592.0001599

Liu J, Liu YJ, Bai YX, et al., 2020b. Regional variation and zoning of temperature gradient pattern of concrete box girder. *China Journal of Highway and Transport*, 33(3): 73-84 (in Chinese). https://doi.org/10.3969/j.issn.1001-7372.2020.03.007

Lou P, Zhu JP, Dai GL, et al., 2018. Experimental study on bridge-track system temperature actions for Chinese high-speed railway. *Archives of Civil and Mechanical Engineering*, 18(2):451-464. https://doi.org/10.1016/j.acme.2017.08.006

Lu CF, Cai CX, 2019. Challenges and countermeasures for construction safety during the Sichuan-Tibet railway project. *Engineering*, 5(5):833-838. https://doi.org/10.1016/j.eng.2019.06.007

Ma WQ, Ma YM, Su B, 2011. Feasibility of retrieving land surface heat fluxes from ASTER data using SEBS: a case study from the Namco area of the Tibetan plateau. *Arctic, Antarctic, and Alpine Research*, 43(2):239-245. https://doi.org/10.1657/1938-4246-43.2.239

Meng QL, Zhu JS, 2018. Fine temperature effect analysis-based time-varying dynamic properties evaluation of long-span suspension bridges in natural environments. *Journal of Bridge Engineering*, 23(10):04018075. https://doi.org/10.1061/(ASCE)BE.1943-5592.0001279

MOT (Ministry of Transport of the People's Republic of China), 2015. General Specifications for Design of Highway Bridges and Culverts, JTG D60-2015. MOT, Beijing, China (in Chinese).

Niu FJ, Xu J, Lin ZJ, et al., 2008. Permafrost characteristics of the Qinghai-Tibet plateau and methods of roadbed construction of railway. *Acta Geologica Sinica*, 82(5):949-958. https://doi.org/10.1111/j.1755-6724.2008.tb00650.x

NMIC (National Meteorological Information Center), 2021. Daily Meteorological Dataset of Basic Meteorological Elements of China National Surface Weather Station (V3.0). NMIC, Beijing, China (in Chinese).

NRA (National Railway Administration of the People's Republic of China), 2017. Code for Design of Concrete Structures of Railway Bridge and Culvert, TB 10092-2017. NRA, Beijing, China (in Chinese).

Razali NM, Wah YB, 2011. Power comparisons of Shapiro-Wilk, Kolmogorov-Smirnov, Lilliefors and Anderson-Darling tests. *Journal of Statistical Modeling and Analytics*, 2(1):21-33.

Royston P, 1992. Approximating the Shapiro-Wilk W-test for non-normality. *Statistics and Computing*, 2(3):117-119. https://doi.org/10.1007/BF01891203

Sheng XW, Zheng WQ, Zhu ZH, et al., 2019. Solar radiation time-varying temperature field and temperature effect on small radius curved rigid frame box girder bridge. *Journal of Traffic and Transportation Engineering*, 19(4): 24-34 (in Chinese). https://doi.org/10.3969/j.issn.1671-1637.2019.04.003

Sheng XW, Yang Y, Zheng WQ, et al., 2020a. Study on the time-varying temperature field of small radius curved concrete box girder bridges. *AIP Advances*, 10(10):105013. https://doi.org/10.1063/1.5133992

Sheng XW, Zheng YH, Zheng WQ, et al., 2020b. Vertical temperature gradient model of concrete box girders based on real-time shadow technology. *Journal of South China University of Technology (Natural Science Edition)*, 48(10): 40-47 (in Chinese). https://doi.org/10.12141/j.issn.1000-565X.190279

Song L, Liu HB, Cui CX, et al., 2020. Thermal deformation and interfacial separation of a CRTS II slab ballastless track multilayer structure used in high-speed railways based on meteorological data. *Construction and Building Materials*, 237:117528. https://doi.org/10.1016/j.conbuildmat.2019.117528

Song ZW, Xiao JZ, Shen LM, 2012. On temperature gradients in high-performance concrete box girder under solar radiation. *Advances in Structural Engineering*, 15(3): 399-415. https://doi.org/10.1260/1369-4332.15.3.399

Tan WD, Gan FF, Chang TC, 2004. Using normal quantile plot to select an appropriate transformation to achieve normality. *Computational Statistics & Data Analysis*, 45(3): 609-619. https://doi.org/10.1016/S0167-9473(03)00009-4

Tayşi N, Abid S, 2015. Temperature distributions and variations in concrete box-girder bridges: experimental and finite element parametric studies. *Advances in Structural Engineering*, 18(4):469-486. https://doi.org/10.1260/1369-4332.18.4.469

Tong M, Tham LG, Au FTK, 2002. Extreme thermal loading on steel bridges in tropical region. *Journal of Bridge Engineering*, 7(6):357-366. https://doi.org/10.1061/(asce)1084-0702(2002)7:6(357)

Wang LM, 2013. Research on Thermal Diffusion Process of Asphlat Paving and Mix Improvement at Low Temperature. PhD Thesis, Harbin Institute of Technology, Harbin, China (in Chinese).

Xue YG, Kong FM, Li SC, et al., 2021. China starts the world's hardest "Sky-High Road" project: challenges and countermeasures for Sichuan-Tibet railway. *The Innovation*, 2(2):100105. https://doi.org/10.1016/j.xinn.2021.100105

Zeng ZP, Huang ZB, Yin HT, et al., 2018. Influence of track line environment on the temperature field of a double-block ballastless track slab. *Advances in Mechanical Engineering*, 10(12):1-16. https://doi.org/10.1177/1687814018812325

Zhang CY, Liu YJ, Liu J, et al., 2020. Validation of long-term temperature simulations in a steel-concrete composite girder. *Structures*, 27:1962-1976. https://doi.org/10.1016/j.istruc.2020.07.070

Zhou GD, Yi TH, 2013. Thermal load in large-scale bridges: a state-of-the-art review. *International Journal of Distributed Sensor Networks*, 9(12):217983. https://doi.org/10.1155/2013/217983

Zhou GD, Yi TH, Chen B, et al., 2015. Analysis of three-dimensional thermal gradients for arch bridge girders using long-term monitoring data. *Smart Structures and Systems*, 15(2):469-488. https://doi.org/10.12989/sss.2015.15.2.469